Evolution of the Dinuclear System in Fission, Quasifission, Incomplete and Complete Fusion

G. G. Adamian[1], A. V. Andreev[1], N. V. Antonenko[1], Sh. A. Kalandarov[1], W. Scheid[2], and A. S. Zubov[1]

[1] Joint Institute for Nuclear Research, 141980 Dubna, Moscow Region, Russia
[2] Institut für Theoretische Physik der Justus-Liebig-Universität, Giessen, Germany

Abstract. The dynamics of fission and fusion is described by the dinuclear system concept which assumes two touching nuclei which carry out motion in the internuclear distance and exchange nucleons by transfer. The corresponding model is applied to obtain fission and quasifission distributions and to calculate evaporation residue cross sections for complete and incomplete fusion reactions leading to superheavy nuclei.

1 Introduction

The time evolution of the nuclear system in fission, quasifission, incomplete and complete fusion reactions can be described with the dinuclear system concept [1,2]. This concept was introduced by V. V. Volkov [2]. A dinuclear system (DNS) or nuclear molecule consists of a configuration of two touching nuclei (clusters) which keep their individuality. Such a system has two main degrees of freedom which govern its dynamics: (i) the relative motion between the nuclei describing molecular resonances in the internuclear potential and the decay of the dinuclear system which is called quasifission and (ii) the transfer of nucleons between the nuclei leading to a dependence of the dynamics on the mass and charge asymmetries in fusion and fission reactions. The latter processes are described by the mass and charge asymmetry coordinates

$$\eta = \frac{A_1 - A_2}{A_1 + A_2} \quad \text{and} \quad \eta_Z = \frac{Z_1 - Z_2}{Z_1 + Z_2}. \tag{1}$$

These coordinates can be assumed as continuous or discrete quantities. For $\eta = \eta_Z = 0$ we have a symmetric clusterization with two equal nuclei, and if η approaches the values ± 1 or if A_1 or A_2 is equal to zero, a compound nucleus has been formed.

According to the dinuclear system concept, the transfer of nucleons between the nuclei plays an important role for fusion and fission. The potential is of diabatic type in the internuclear distance with a minimum in the touching range and a repulsive part towards smaller relative distances prohibiting the dinuclear system to amalgamate to the compound nucleus in the relative coordinate. Such a potential can be calculated with a dynamical diabatic two-center shell model [3] and has a survival time of the order of the reaction time of 10^{-20} s. It can also be justified with structure

calculations based on group theoretical methods [4]. Also a coordinate-dependence of the mass of relative motion between the nuclei leads to an energy-dependent repulsive potential after the transformation to a constant mass. Then the outer range of the potential is screened from the inner one and, therefore, this potential has similar properties as the diabatic one [5].

In this article we review some aspects of the DNS model in its application to fission and fusion and present recent results for evaporation residue cross sections. We like to mention that the DNS model has a large variety of applications also in nuclear structure physics [6–9]. For example, it is used for the description of normal-, super- and hyperdeformed bands in deformed nuclei.

2 Binary and ternary fission

Bimodal and multimodal binary fission can be described on the basis of the potential energy surface of the dinuclear system model and extended to ternary fission [10, 11]. The fissioning nucleus with mass and charge numbers A and Z, respectively, is described at the scission point as a dinuclear system (DNS) with two fission fragments in contact. Typical characteristics of the DNS are the excitation energy E^*, the mass (A_L, $A_H = A - A_L$) and charge (Z_L, $Z_H = Z - Z_L$) numbers and the deformation parameters (β_L, β_H) of light (L) and heavy (H) DNS fragments. The fragment pairs are nearly touching, coaxial prolate ellipsoids. The deformation parameters β_L and β_H are defined as the ratios of the major and minor semiaxes of the ellipsoids. The potential energy is the sum of the liquid-drop and shell correction energies of each DNS nucleus and of the Coulomb and nuclear potential terms describing the interaction between the nuclei. The excitation energy is assumed to be distributed between the fragments proportional to their masses.

In Fig. 1 we show the potential energies of scission configurations as functions of β_L and β_H for the neutron-induced fission of ^{236}U leading to ^{104}Mo + ^{132}Sn and ^{104}Zr + ^{132}Te. The minima in the potential energy surface determine the most probable fission configurations. The relative primary (before evaporation of neutrons) yields Y of fission fragments are calculated in the framework of the statistical treatment:

$$Y(\{A_i, Z_i, \beta_i\}) = Y_0 \exp\left(-U(\{A_i, Z_i, \beta_i\}, R_b, E^*)/T\right) \tag{2}$$

with the normalization factor Y_0. Here, $T = (E^*/a)^{1/2}$ with $a = A/12$ MeV^{-1} is the temperature at that scission configuration which has the minimal potential energy among the configurations considered. The secondary (after evaporation of neutrons) yields of fission fragments are obtained by using the excitation energies of the fragments which consist of the excitation energies of the fragments at scission and the deformation energies transferred into the internal excitation energies after scission.

Figure 2 shows the kinetic energy and mass distributions of fission fragments of ^{258}Fm and ^{258}No where the kinetic energy distribution is approximated by Gaus-

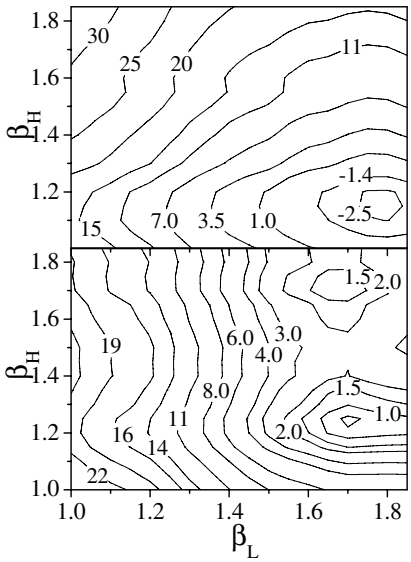

Figure 1. Potential energy of scission configurations as functions of β_L and β_H for the neutron induced fission of ^{236}U leading to ^{104}Mo + ^{132}Sn (upper part) and ^{104}Zr + ^{132}Te (lower part).

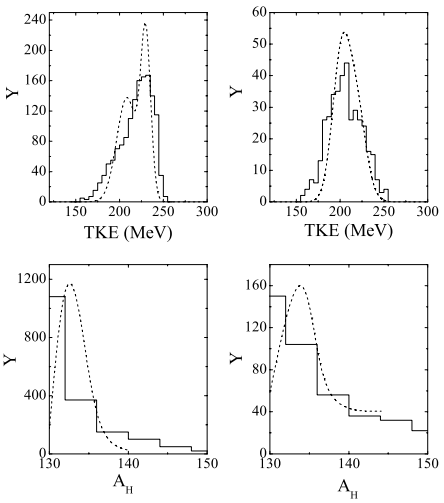

Figure 2. The calculated (dashed curves) kinetic energy distribution (upper part) and mass distribution (lower part) of fission fragments of ^{258}Fm (left part) and ^{258}No (right part) are compared with experimental data (histogram).

sians for the scission configurations determined by the minima in the potential energy surface. The experimental data agree satisfactorily with the calculated distributions.

With the same procedure one can treat the ternary fission [11]. The ternary system consists of two prolate coaxial ellipsoidal heavy fragments and a light charged particle (LCP), where the LCP is formed in the region between the two heavy fragments. The potential energy surfaces for different ternary systems are calculated as functions of the deformations of the two heavy fragments. Usually there are less minima in the potential energy surfaces in comparison with binary systems since the distance between the heavy fragments is larger than that in the binary case. The binary system is firstly formed and then the ternary system arises by extracting the LCP, consisting of one or several alpha-particles and neutrons, from one or both binary fragments. The ternary system can not be directly formed from the compound nucleus because a potential barrier between the binary and ternary fission valleys prevents the straight formation of the ternary system. In this picture the charge distribution for ternary fission is strongly ruled by the one for binary fission.

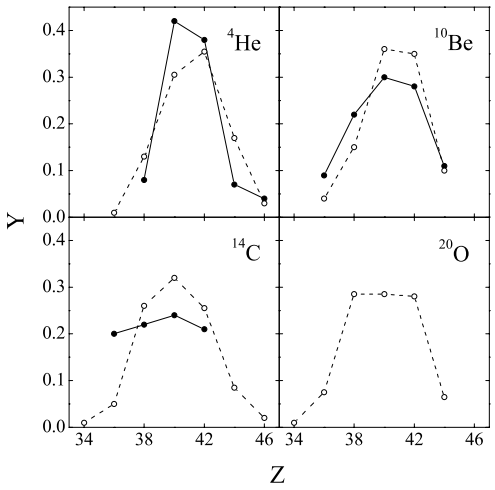

Figure 3. Charge distributions in spontaneous ternary fission of ^{252}Cf with different LCPs. The calculated and experimental points are shown by empty and filled circles, respectively, connected by straight lines.

The relative probabilities for the formation of different binary systems are calculated with the above expression. From each binary system several ternary systems can be formed with relative probabilities again obtained with an analogous expression and normalized to unity for each binary system. An example of our calculations is shown in Fig. 3 for the ternary fission of ^{252}Cf and compared with experimental data.

3 Evaporation residue cross section

The cross section for the production of superheavy nuclei can be written

$$\sigma_{ER}(E_{c.m.}) = \sum_{J=0}^{J_{max}} \sigma_{cap}(E_{c.m.}, J) P_{CN}(E_{c.m.}, J) W_{sur}(E_{c.m.}, J). \qquad (3)$$

The three factors are the capture cross section, the probability for complete fusion and the survival probability. The maximal contributing angular momentum J_{max} is of the order of 10 - 15. The capture cross section σ_{cap} describes the formation of the dinuclear system at the initial stage of the reaction when the kinetic energy of the relative motion is transferred into potential and excitation energies. The DNS can decay by crossing the quasifission barrier B_{qf} which is of the order of 0.5 - 5 MeV.

After its formation the DNS evolves in the mass asymmetry coordinate. The center of the mass distribution moves towards more symmetric fragmentations and its width is broadened by diffusion processes. The part of the distribution, which crosses the inner fusion barrier B^*_{fus} of the driving potential $U(\eta)$, yields the probability P_{CN} for complete fusion. The DNS can also decay by quasifission during its evolution. Therefore, the fusion probability P_{CN} and the mass and charge distributions of the quasifission have to be treated simultaneously.

The fusion probability can be quantitatively estimated with the Kramers formula and results as

$$P_{CN} \sim \exp(-(B^*_{fus} - \min[B_{qf}, B_{sym}])/T), \qquad (4)$$

where the temperature T is related to the excitation energy of the DNS, and B_{sym} is the barrier in η to more symmetric configurations. B_{sym} is 4-5 MeV ($> B_{qf}$) in cold fusion reactions and 0.5-1.5 MeV ($< B_{qf}$) in hot fusion reactions. Since the inner fusion barrier increases with decreasing mass asymmetry, we find an exponential depression of the fusion probability towards symmetric projectile and target combinations in lead based reactions. In hot fusion reactions with ^{48}Ca projectiles, P_{CN} drops down with increasing mass and charge of the target nucleus. These systems run easier towards symmetric fragmentations and undergo quasifission there.

The excited compound nucleus decays by fission and emits neutrons besides negligible emissions of other particles and photons. The probability to reach the ground state of the superheavy nucleus by neutron emission is denoted as survival probability W_{sur}. In the case of the one-neutron emission in Pb-based reactions the survival probability is roughly the ratio Γ_n/Γ_f of the widths for neutron emission and for fission because of $\Gamma_f \gg \Gamma_n$. The survival probability depends sensitively on the nuclear structure properties of the superheavy nuclei like on the level density, fission barriers and deformation [12].

With the DNS concept we reproduced the measured evaporation residue cross sections of the Pb- and actinide-based reactions with a precision of a factor of two. Figure 4 shows examples for cold and hot fusion reactions [13, 14]. These calculations are very valuable and support an adequate choice of projectile and target nuclei in experiment.

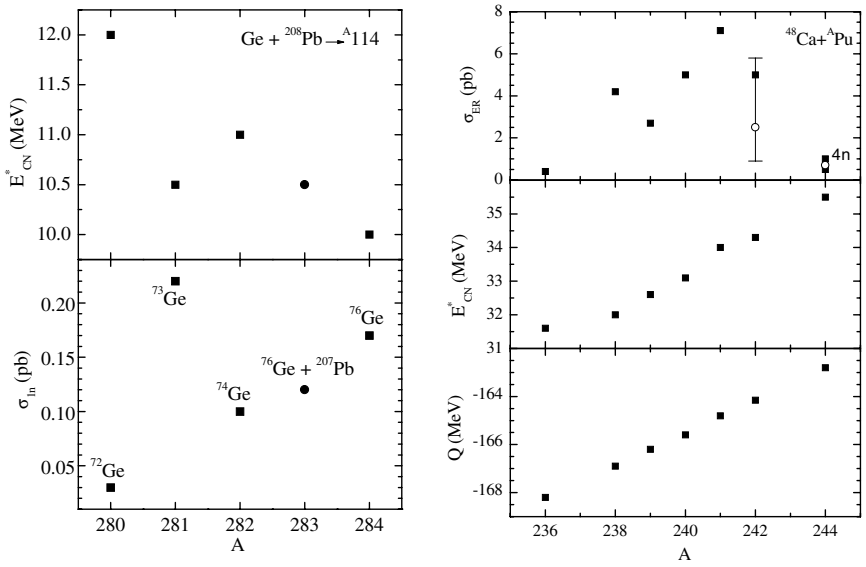

Figure 4. Excitation energy E^*_{CN}, evaporation residue cross section σ_{1n}, $\sigma_{3n,4n}$ and Q-value for Ge + ^{208}Pb $\rightarrow$ $^{A}114$ (l.h.s.) and ^{48}Ca + ^{A}Pu $\rightarrow$ 114 (r.h.s.). The experimental points are from Ref. [16].

4 Master equations for nucleon transfer

The dynamics of mass and charge transfer, the fusion and the succeeding quasifission can be studied with master equations [15]. At the starting point we consider the shell model Hamiltonian of all dinuclear fragmentations of the nucleons. This Hamiltonian can be used to derive master equations for the probability $P_{Z,N}(t)$ to find the dinuclear system in a fragmentation with $Z_1 = Z$, $N_1 = N$ and $Z_2 = Z_{tot} - Z_1$, $N_2 = N_{tot} - N_1$. The master equations are

$$\begin{aligned}\frac{d}{dt}P_{Z,N}(t) &= \Delta^{(-,0)}_{Z+1,N}P_{Z+1,N}(t) + \Delta^{(+,0)}_{Z-1,N}P_{Z-1,N}(t) \\ &+\Delta^{(0,-)}_{Z,N+1}P_{Z,N+1}(t) + \Delta^{(0,+)}_{Z,N-1}P_{Z,N-1}(t) \\ &- \left(\Delta^{(-,0)}_{Z,N} + \Delta^{(+,0)}_{Z,N} + \Delta^{(0,-)}_{Z,N} + \Delta^{(0,+)}_{Z,N}\right) P_{Z,N}(t) - \Lambda^{qf}_{Z,N}P_{Z,N}(t). \qquad (5)\end{aligned}$$

The one-proton and one-neutron transfer rates $\Delta^{(.,.)}$ depend on the single particle energies and the temperature of the DNS. The occupation of the single particle states is taken into account by a Fermi distribution. The simultaneous transfer of more nucleons is neglected. The quantity $\Lambda^{qf}_{Z,N}$ is the rate for quasifission in the internuclear coordinate R and is calculated with the Kramers formula. This rate causes a loss of

the total probability $\sum_{Z,N} P_{Z,N}(t) \leq 1$. The DNS dynamics was also studied by Li *et al.* [17] with similar master equations.

The fusion probability is given by

$$P_{CN} = \sum_{Z<Z_{BG},N<N_{BG}} P_{Z,N}(t_0). \tag{6}$$

It is the fraction of probability existing for $Z < Z_{BG}$ and $N < N_{BG}$ at the reaction time t_0, where Z_{BG} and N_{BG} determine the fusion barrier in the charge and neutron asymmetry coordinates. The reaction time is $t_0 \approx (3-5) \times 10^{-20}$ s and is determined by solving the balance equation for the probabilities. The DNS with $Z < Z_{BG}$ and $N < N_{BG}$ evolves to the compound nucleus in a time of 10^{-21}s which is short compared with the decay time of the compound nucleus.

The mass and charge yields for quasifission are obtained as

$$Y(A_1) = \sum_{Z_1} \int_0^{t_0} \Lambda^{qf}_{Z_1,A_1-Z_1} P_{Z_1,A_1-Z_1}(t)\, dt, \tag{7}$$

$$Y(Z_1) = \sum_{N_1} \int_0^{t_0} \Lambda^{qf}_{Z_1,N_1} P_{Z_1,N_1}(t)\, dt. \tag{8}$$

The process of quasifission which is the decay of the DNS leads to a large quantity of observable data like mass and charge distributions, distributions of total kinetic energies (TKE), variances of total kinetic energies and neutron multiplicities. Therefore, the comparison of the theoretical description with experimental data provides sensitive information about the applicability and correctness of the used model. We calculated quasifission distributions, TKEs, variances of TKE and neutron multiplicities for cold and hot fusion reactions [15] and found satisfying agreement with the experimental data of Itkis *et al.* [18].

4.1 Production of asymmetric systems accompanying fusion reactions

The master equations also give probabilities for more asymmetric systems than the initial one. The cross section $\sigma(Z,N)$ for the production of a primary heavy nucleus in the asymmetric-exit-channel quasifission can be calculated as follows:

$$\sigma(Z = Z_{tot} - Z_1, N = N_{tot} - N_1) = \sigma_{cap} Y(Z,N) \tag{9}$$
$$\text{with} \qquad Y(Z,N) = \int_0^{t_0} \Lambda^{qf}_{Z_1,N_1} P_{Z_1,N_1}(t)\, dt.$$

The capture cross section is estimated as $\sigma_{cap} = \pi\hbar^2 J_{cap}(J_{cap}+1)T/(2\mu E_{c.m.})$ with $J_{cap} = 20$. Here, T is the penetrability through the Coulomb barrier which is set about 0.5 at $E_{c.m.}$ near the barrier and 1 for larger values of $E_{c.m.}$.

In Fig. 5 we present production (transfer) cross sections for asymmetric fragmentations in the reactions ^{70,72,74,76}Ge + ^{208}Pb [19]. The measurement of these

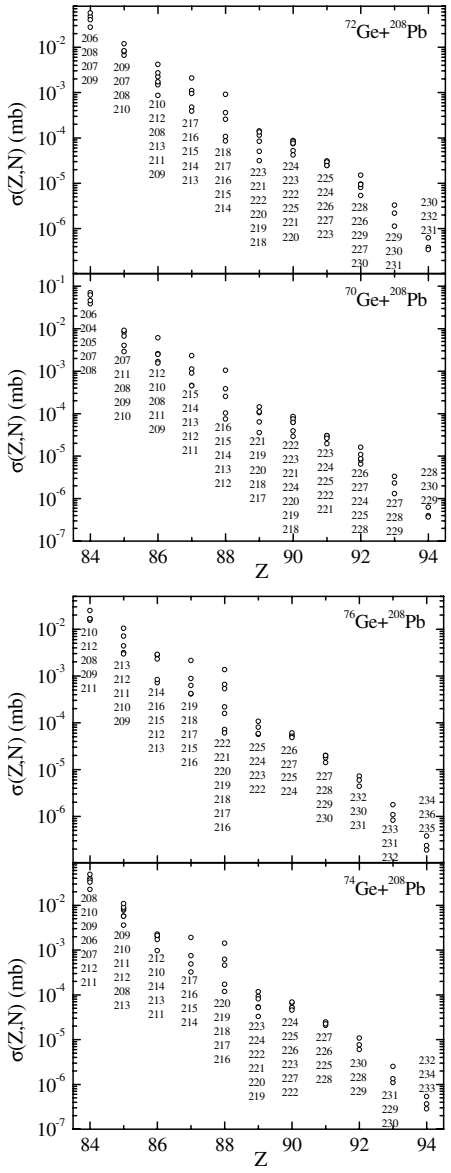

Figure 5. Calculated production cross section in the reactions ^{70,72,74,76}Ge + ^{208}Pb at $E_{c.m.}$ = 267.3, 270.3, 271.3 and 272.3 MeV, respectively, as a function of Z and A of the heavier fragment.

observable cross sections would be a proof for the fusion dynamics in the dinuclear system concept. The incident energies correspond to the expected maxima of the excitation functions of complete fusion for the $1n$ evaporation channel. The yields

of products near the initial DNS increase with decreasing neutron number because of the smaller values of B_{qf}.

Figure 6 shows theoretical evaporation residue cross sections in the reactions ^{48}Ca+^{244,246,248}Cm for the production of heavy nuclei in the asymmetric-exit-channel quasifission with one neutron evaporated [20]. These cross sections are calculated as $\sigma_{ER}(Z, N-x) = \sigma(Z, N)W_{sur}(xn)$. The probabilities $Y(Z, N)$ in Fig. 6 are estimated with master equations and a Kramers-type formula for the quasi-fission rate. One can produce new isotopes of superheavy nuclei with $Z = 104-108$ which fill the gap between the isotopes of heaviest nuclei obtained in cold and hot complete fusion reactions.

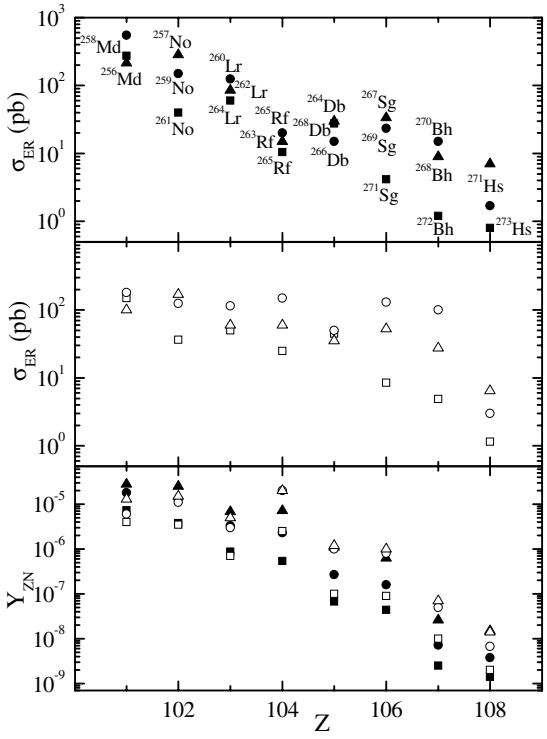

Figure 6. Calculated primary yields (lower part) and evaporation residue cross sections (middle and upper parts) are shown by triangles, circles and squares for the reactions ^{48}Ca + ^{244,246,248}Cm ($E_{c.m.}$=207, 205.5 and 204 MeV), respectively. The heavy fragments after $1n$ evaporation are indicated in the upper part of the figure. The closed and open symbols are calculated with the master equations and Kramers-type formula, respectively.

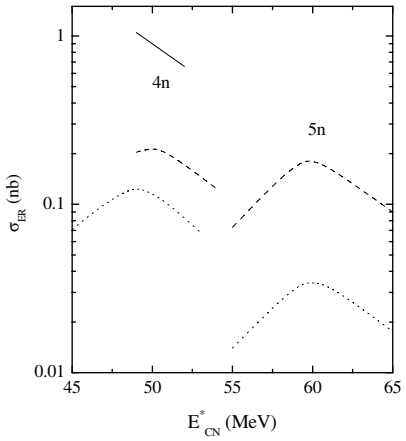

Figure 7. Calculated excitation functions of the evaporation residue cross sections for the indicated xn evaporation channels in the reactions ^{40}Ca + ^{184}W (solid curve), ^{40}Ca + ^{186}W (dashed curves) and ^{44}Ca + ^{184}W (dotted curves).

4.2 Complete fusion reactions

The master equations are used to calculate the probability P_{CN} for complete fusion. We studied the production of neutron-deficient isotopes of Pu and Cm in complete fusion reactions. In Fig. 7 we show calculated excitation functions of the evaporation residue cross sections for various xn evaporation channels in the reactions ^{40,44}Ca + ^{184,186}W [21]. In these reactions the isotopes $^{220-224}$Pu are produced with rather large cross sections of 0.1 – 1 nb.

Table 1. The calculated evaporation residue cross sections in the indicated most probable channels of the reactions ^{86}Kr+^{134,138}Ba are compared with recent experimental data of Satou *et al.* [22].

Reaction	$\mathbf{E}_{\mathrm{c.m.}}$ (MeV)	Channels	$\sigma^{\mathbf{th}}_{\mathbf{ER}}$ (nb)	$\sigma^{\mathbf{exp}}_{\mathbf{ER}}$ (nb)
^{86}Kr+^{138}Ba	213.3	$\underline{n} + \alpha n + 2\alpha n$	14	20^{+15}_{-12}
	218.6	$n + \underline{\alpha n} + 2\alpha n$	18	8^{+10}_{-6}
	225.3	$n + \alpha n + \underline{2\alpha n}$	94	50^{+42}_{-32}
	225.3	$2n + \underline{\alpha 2n} + 2\alpha 2n$	59	19^{+38}_{-19}
	232.3	$2n + \underline{\alpha 2n} + 2\alpha 2n$	64	140^{+120}_{-90}
	237.4	$3n + \underline{\alpha 3n}$	156	180^{+130}_{-100}
^{86}Kr+^{134}Ba	220	$2n + \underline{\alpha 2n}$	1	2^{+5}_{-2}
	220.9	$np + \underline{\alpha np}$	0.7	6^{+12}_{-6}
	227	$np + \underline{\alpha np}$	1.7	6^{+13}_{-6}
	229	$np + \underline{\alpha np}$	3	

For comparison with experimental data we give results of calculations with master equations for the fusion reactions ^{86}Kr+^{134,138}Ba in Table 1. Near the maxima of the excitation functions, the agreement of the theoretical results and experimental data is quite good. Note that in the experiment [22] not all channels are separated and the error bars are rather large.

Acknowledgments

We thank DFG (Bonn), VW-Stiftung (Hannover) and RFBR (Moscow) for supporting this work. We thank Prof. Junqing Li (Lanzhou), Prof. Enguang Zhao (Beijing), Prof. Shangui Zhou (Beijing), Prof. Wei Zuo (Lanzhou) and Dr. Ning Wang (Giessen) for valuable discussions and help.

References

1. G. G. Adamian, N. V. Antonenko, W. Scheid, and V. V. Volkov, *Nucl. Phys.* **A633**, 409 (1998).
2. V. V. Volkov, *Izv. AN SSSR ser. fiz.* **50**, 1879 (1986).
3. A. Diaz-Torres, G. G. Adamian, N. V. Antonenko, and W. Scheid, *Phys. Lett.* **B481**, 228 (2000).
4. G. G. Adamian, N. V. Antonenko, and Yu. M. Tchuvil'sky, *Phys. Lett.* **B451**, 289 (1999).
5. H. J. Fink, W. Scheid, and W. Greiner, *J. Phys. G (Nucl. Phys.)* **1**, 685 (1975).
6. T. M. Shneidman, G. G. Adamian, N. V. Antonenko, S. P. Ivanova, and W. Scheid, *Nucl. Phys.* **A671**, 119 (2000).
7. G. G. Adamian, N. V. Antonenko, R. V. Jolos, Yu. V. Palchikov, and W. Scheid, *Phys. Rev.* **C67**, 054303 (2003).
8. G. G. Adamian, N. V. Antonenko, R. V. Jolos, Yu. V. Palchikov, W. Scheid, and T. M. Shneidman, *Phys. Rev.* **C69**, 054310 (2004).
9. G. G. Adamian, N. V. Antonenko, N. Nenoff, and W. Scheid, *Phys. Rev.* **C64**, 014306 (2001).
10. A. V. Andreev, G. G. Adamian, N. V. Antonenko, and S. P. Ivanova, *Eur. Phys. J.* **A26**, 327 (2005).
11. A. V. Andreev, G. G. Adamian, N. V. Antonenko, S. P. Ivanova, S. N Kuklin, and W. Scheid, *Eur. Phys. J.* **A30**, 579 (2006).
12. A. S. Zubov, G. G. Adamian, N. V. Antonenko, S. P. Ivanova, and W. Scheid, *Eur. Phys. J.* **A23**, 249 (2005).
13. G. G. Adamian, N. V. Antonenko, and W. Scheid, *Phys. Rev.* **C69**, 011601 (2004).
14. G. G. Adamian, N. V. Antonenko, and W. Scheid, *Phys. Rev.* **C69**, 014607 (2004).
15. G. G. Adamian, N. V. Antonenko, and W. Scheid, *Phys. Rev.* **C68**, 034601 (2003).
16. Yu. Ts. Oganessian *et al.*, *Eur. Phys. J.* **A13**, 135 (2002); **A15**, 201 (2002).
17. W. Li, N. Wang, J. F. Li, H. Xu, W. Zuo, E. Zhao, J. Q. Li, and W. Scheid, *Europhys. Lett.* **64**, 750 (2003).
18. M. G. Itkis *et al.*, *Nucl. Phys.* **A734**, 136 (2004).
19. G. G. Adamian and N. V. Antonenko, *Phys. Rev.* **C72**, 064617 (2005).
20. G. G. Adamian, N. V. Antonenko, and A. S. Zubov, *Phys. Rev.* **C71**, 034603 (2005).
21. G. G. Adamian, N. V. Antonenko, S. P. Ivanova, W. Scheid, and A. S. Zubov, *to be published* (2007).
22. K. Satou *et al.*, *Phys. Rev.* **C73**, 034609 (2006).